Enhanced electrochemical water splitting activity in annealed TiO2 nanoparticles of photoanode

Tien Thanh Nguyen (ntthanh@ims.vast.ac.vn)
Vietnam Academy of Science and Technology https://orcid.org/0000-0003-3737-3065
Khac An Dao
Vietnam Academy of Science and Technology
Xuan Dien Luong
Hanoi University of Science and Technology School of Chemical Engineering
Thi Dieu Thuy Ung
Vietnam Academy of Science and Technology

Research Article

Keywords: TiO2, Thermal annealing, Photocatalyst, Water splitting

Posted Date: May 28th, 2021

DOI: https://doi.org/10.21203/rs.3.rs-550425/v1

Enhanced electrochemical water splitting activity in annealed TiO_2 nanoparticles of photoanode

Tien Thanh Nguyen[1,2,*], Khac An Dao[3,1,*], Xuan Dien Luong[4] and Thi Dieu Thuy Ung[1]

[1]*Institute of Materials Science, Vietnam Academy of Science and Technology, 18 Hoang Quoc Viet, Cau Giay, Hanoi, Vietnam*

[2]*Graduate University of Science and Technology, Vietnam Academy of Science and Technology, 18 Hoang Quoc Viet, Cau Giay, Hanoi, Vietnam*

[3]*Institute of Theoretical and Applied Research (ITAR), Duy Tan University, Trang An Complex, Cau Giay, Hanoi, Vietnam*

[4]*School of Chemical Engineering, Hanoi University of Science and Technology, 1 Dai Co Viet, Hanoi, Vietnam*

Abstract

In this paper, we present the electrochemical water splitting characteristics of TiO_2/FTO electrodes via spin-coating method. By using thermal annealing approach, the TiO_2 nanoparticle (P25) was modified with a more active photocatalyst. The annealed TiO_2 nanoparticle-based photoanode in vacuum shows photocurrent density of 0.27 mA/cm^2 and photoconversion efficiency of (η = 0.22%) at potential of 0.4 *V* (*vs. RHE*), which are higher than those of annealed TiO_2 nanoparticle-based electrode in air. The improved photoelectrochemical property is attributed to high oxygen vacancy density with more active sides, while TiO_2 nanoparticle was annealed in vacuum (~10^{-1} torr) with oxide concentration conditions. From this finding, we propose that a thermal annealing process might serve as an approach for fabricating the photoanodes of TiO_2-based materials consisting of much active photocatalyst

Keywords: TiO_2, Thermal annealing, Photocatalyst, Water splitting

[*] Corresponding author, email; ntthanh@ims.vast.ac.vn; andaokhac@gmail.com

1. Introduction

In the past, metal oxide (MO) materials and their composites have been attracting much attention from the research community in terms of photocatalytic splitting of water using sunlight [1-5]. Various MO (TiO_2, WO_3, CuO, Fe_2O_3, In_2O_3, and $BiVO_4$) structures and morphology engineering for photoelectrochemical (PEC) devices are of interest to obtain a great product of H_2 and O_2 gases [6-10]. Even though traditional MOs for splitting water have been known for decades, recently the PEC systems were synthesized by a hybrid of MO and other semiconductors. Among them, crystalline anatase TiO_2 [2, 11] is distorted octahedral coordination (O_h), which consists of more active sites than other phases (rutile (D_{2h}) and brookite). An efficient PEC water splitting system has been developed due to useful properties such as an *n*–type semiconductor, high photoconversion efficiency, long-term stability, large density of states in the conduction band derived from the d–orbital, inexpensive cost, earth-abundant, environmentally friendly issues for device fabrication [12, 13]. In general, electrons photoexcited in the valence band of TiO_2 are sufficiently energetic to be transferred to the water for H_2 production. However, the high recombination rate of carrier pairs, non-Schottky contact, and large bandgap (*ca.* 3.2 eV) issues of as-synthesized TiO_2 reduce the generated photocurrent of the PEC device [14-18]. Thus, photocatalytic water-splitting using anatase TiO_2 for high H_2 production has been of interest to scientists. Based on those issues, many efforts to fabricate TiO_2-based PEC devices for H_2 production were reported such as structure engineering [6, 19], noble metal loading/doping [14, 5, 18], modified oxygen vacancy density [20, 21], and enhanced localized surface plasmon resonance [22-

24] approaches. Among them, the preparation of anatase TiO_2 phase with modified oxygen vacancy and large surface area has attracted much attention in terms of increasing the active photocatalytic properties compared to other phases. Because it has been vastly used as an overall efficient photocatalyst, and stable for PEC application [3, 14, 25, 5, 9, 17, 26]. Therefore, many techniques have been done to synthesize anatase TiO_2 phase for water splitting application, including hydrothermal/ solvothermal [27, 19, 28], oxidation [29, 19, 28], thermal plasma [30, 28], electrophoretic deposition [31, 32, 28], sol-gel [33, 34, 28], spray pyrolysis [35, 28] methods. However, the mechanism of TiO_2-based water splitting is not clearly known, there are still many limitations affecting the PEC performance [3, 34]. In this work, thus, we consider the preparation of TiO_2 nanoparticle-based photoanode using commercial TiO_2 nanoparticles (P25) by the spin-coating approach. TiO_2 nanoparticle is annealed at a temperature of 450 ^oC in air/vacuum ($\sim 10^{-1}$ torr) for 100 min. By manipulating annealing conditions, the effect of annealing conditions on the crystalline structure, morphology, optical properties of TiO_2 material was investigated. Based on this result, we studied the PEC water splitting characteristics of the TiO_2 photoanode using an electrolyte (Kpi phosphate buffer solution, 1.0 M KH_2PO_4/K_2HPO_4, $pH = 7$). This annealing method paves the way for the fabrication of the TiO_2 material-based PEC device with a more active photocatalyst.

2. Experiments

The materials (TiO_2 nanoparticles, P25) and fluorine-doped tin oxide substrate (FTO, TEC glass, 1.5 cm × 2.0 cm × 2.0 mm, 7.0 Ω/sp) and chemicals (acetone – CH_3COCH_3,

99.5%), ethanol – C_2H_5OH, 99.5%) were purchased from Alfa Aesar and Sigma Aldrich. A mix of 0.73 mg of TiO_2 nanoparticles was dissolved into 50 ml ethanol for a 1.8% in weight concentration. This solution was stirred for 30 min at room temperature (RT) for a uniform. This solution was deposited on the FTO substrate by the spin-coating technique (with step 1: a 500 rpm for 5 sec, and step 2: a 3000 rpm for 30 sec) three times. Samples were investigated at an annealing temperature of 450 ^oC for 100 min in air (TO-Abi sample) and vacuum (~ 1×10^{-1} torr, TO-Vac sample). The composition of the TiO_2 layer was studied by the energy dispersive X–ray (EDS, Hitachi S4800, Japan). The crystalline structure of TiO_2 film was measured by the Siemen D–5000 X-ray diffractometer using Cu–Kα radiation, λ = 1.546 Å. The optical properties were investigated by a Raman Horiba XploRA Plus, Nicolet iS10, an Agilent Cary 5000 UV/VIS/NIR spectrometer, a Horiba iHR550 spectrometer using a 355 nm pulsed Nd:YAG laser as an excitation source. The photoelectrochemical (PEC) cell with a working area of 0.5 cm × 0.5 cm was made from the TiO_2/FTO/glass substrate using epoxy to cover the undesired area. The PEC characteristic was investigated by a three electrode system (a saturated Ag/AgCl electrode as the reference electrode (in a 3.0 M KCl, CHI instruments), a Pt sheet as the counter, and an FTO/TiO_2 as the working electrode), an electrolyte analyzer (BioLogic SP300 potentiostat) using a Kpi phosphate buffer solution (1.0 M KH_2PO_4/K_2HPO_4, pH = 7) and solar simulation system (PEC-L01 AM 1.5G lam power 100 mW/cm^2, 10 mV.s^{-1}).

3. Results and discussion

Fig. 1 shows XRD patterns of TiO_2 film annealed at 450 °C in air and vacuum for 100 min, indicating ca. 80 wt.% of anatase and 20 wt.% of rutile for TO-Vac sample compared to 81.6 wt.% of anatase and 18.4 wt.% of rutile for TO-Abi sample. The XRD peaks at 2θ = 25.50°, 37.93°, 38.69°, 48.2°, 53.95°, 55.24°, 62.99°, and 69.03° correspond to the atomic planes of (1 0 1), (0 0 4), (1 1 2), (2 0 0), (1 0 5), (2 1 1), (1 1 8), and (1 1 6) anatase TiO_2 according to *JCPDS No. 21-1272*. The peaks at 2θ = 27.53°, 36.25°, and 41.43° are assigned to the atomic planes of (1 1 0), (1 0 1), and (1 1 1) of rutile TiO_2, according to *JCPDS No. 21-1276*.

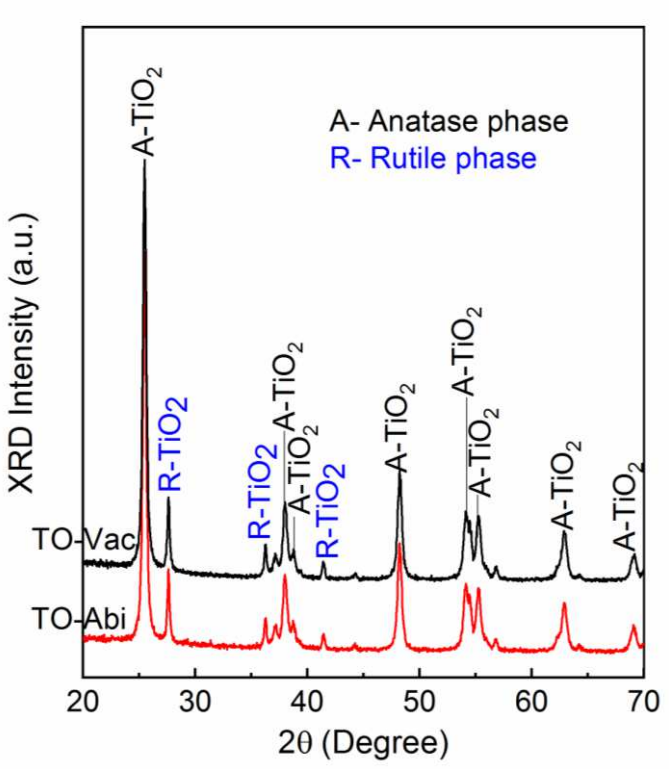

Fig. 1. XRD patterns of the TiO_2 particle annealed at 450 °C in air (TO-Abi sample), and in vacuum (~10^{-1} torr, TO-Vac sample)

The existence of two anatase and rutile phases comes from the mixing phase of the non-completed synthesis process of TiO_2 at low temperature (below 500 ^oC). The number and intensity of XRD peaks of the rutile and anatase phases of both samples are similar. The number of XRD peaks of the rutile phase is less than that of the anatase phase, which is attributed to the dominant phase of the anatine crystal at 450 ^oC. At present, the anatase phase tendency has grown by converting rutile to anatase phase. The phase shift is non-completed, which is original to form high oxygen vacancy (OV) density of the anatine phase. Because OVs of TiO_2 are attributed to reduced energy bandgap of TiO_2 structure [20, 36, 37, 21] that might extend the absorption wavelength range of sunlight for improving the efficiency of PEC device.

Fig. 2 presents the energy dispersive X-ray spectrum (EDS) of TiO_2/FTO/glass film annealed at 450 ^oC in air (TO-Abi sample) and in a vacuum (TO-Vac sample). The spectrum shows that oxygen and titanium elements make up 70.26 and 29.64% in weight, respectively, for the TO-Abi sample, while those elements accounted for 66.92 and 33.08% in weight for the TO-Vac sample, respectively. The oxygen concentration of the TO-Abi sample is higher at 3.34% than that of the TO-Vac sample. We did not obtain the Sn and F elements as well as other contaminations from the FTO substrate. The low oxygen density during the phase process from rutile to anatase causes high OV density of TiO_2 structure, especially at the interface between rutile and anatase phases. Due to the effect of defect density and OV density on bandgap energy of TiO_2 [20, 36, 25, 21], the role of contamination is very important to manipulating physical properties as well as

PEC TiO_2 based application. Thus, the generated activated photocatalyst of OV under illumination strongly affects the efficiency of PEC device, further.

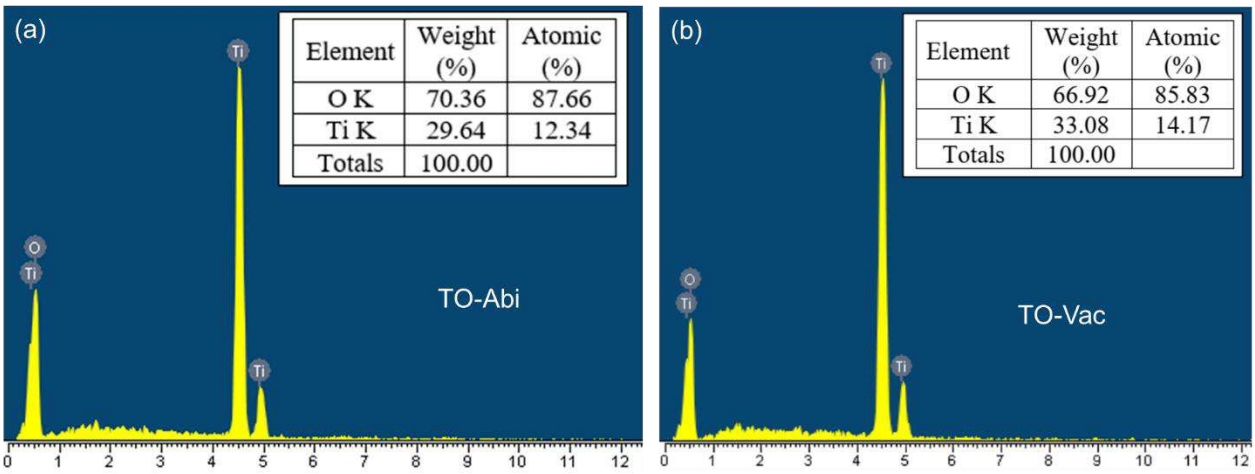

Fig. 2. EDX results of the TiO_2/FTO nanoparticle annealed at temperature of 450 °C for 100 min, (a) TO-Abi sample and (b) TO-Vac sample

Raman spectra of TiO_2/FTO samples annealed at 450 °C in air and vacuum are shown in Fig. 3(a). As can be seen, there are three first order frequency vibrations at $141-\nu_6(E_g)$ cm^{-1}, $195-\nu_5(E_g)\,cm^{-1}$ corresponding to the O–Ti–O bending type Raman, and $635-\nu_1(E_g)\,cm^{-1}$ corresponding to Ti-O stretch bonding Raman, while two phonon frequency peaks at $394-\nu_4(B_{1g})\,cm^{-1}$ and $515-\nu_2/\nu_3(B_{1g}/A_{1g})\,cm^{-1}$ are assigned to Ti–O bond stretching Raman for anatase TiO_2 phase using the 532 nm excitation wavelength. According to the theoretical calculation of space group $D_{4h}^{19}(I4_1/amd)$ [38, 39], the optical phonon (Γ_{opt}) of anatase TiO_2 structure is given by *Equ.* 1

$$\Gamma_{opt} = 1A_{1g} + 1A_{2u} + 2B_{1g} + 1B_{2u} + 3E_g + 2E_u \quad (1)$$

Where E_g (at 144, 197, 640 cm^{-1}), B_{1g} (at 400, 519 cm^{-1}), A_{1g} (at 507 cm^{-1}) are the Raman active modes, and A_{2u} (TO, at 654 cm^{-1}) and E_u (TO, at 169, 643 cm^{-1}) are infrared active modes, and B_{2u} (at 507 cm^{-1}) is the inactive mode of Raman and infrared spectra. The frequencies of anatase TiO_2 from our sample ($E_g(\nu_1,\nu_5,\nu_6)$, $\nu_4(B_{1g})$) are less than calculated frequencies (*ca.* 3 cm^{-1}). This phenomenon is attributed to the effect of insufficient oxygen atoms and many oxygen vacancies in the sublattice of the TiO_2 structure, but this difference is not important. Because main phonon frequencies of anatase TiO_2 phase have still observed that is an oscillation of the compound lattice [38, 39]. Fig. 3(b) shows the Fourier transform infrared (FTIR) spectroscopy of TiO_2/FTO/glass layer at RT in regions between 400 and 4000 cm^{-1}. The results indicated that the spectral FTIR of both samples is stronger sensitive absorption in the short-IR range 400–2000 cm^{-1} than in the mid-IR range (2000–4000 cm^{-1}). There are two main absorption peaks at 1630 cm^{-1} and 3450 cm^{-1} in the IR range that correspond to bending vibration of the H–O–H bond and stretching vibration of the hydroxyl group of the absorbed water molecules. One of the peaks at 1381 cm^{-1} is attributed to the C-OH stretching. The absorption peak located at 3450 cm^{-1} is attributed to isolated OH^- group coordinated with Ti^{4+} atoms. Due to the Ti^{4+} atom charge defect and interaction between hydroxyl groups on TiO_2, the band center is shifted towards a lower wavelength compared to other reports [40-42]. Besides that, the defect chemistry in nonstoichiometric TiO_2 has not been understood for formatting distinct atomic defects

like Ti^{3+}, Ti^{4+}, or oxygen vacancies, according to *Equ. 2* and 3 [25], which are expected to play a crucial role in doping of anatase TiO_2 structure [36].

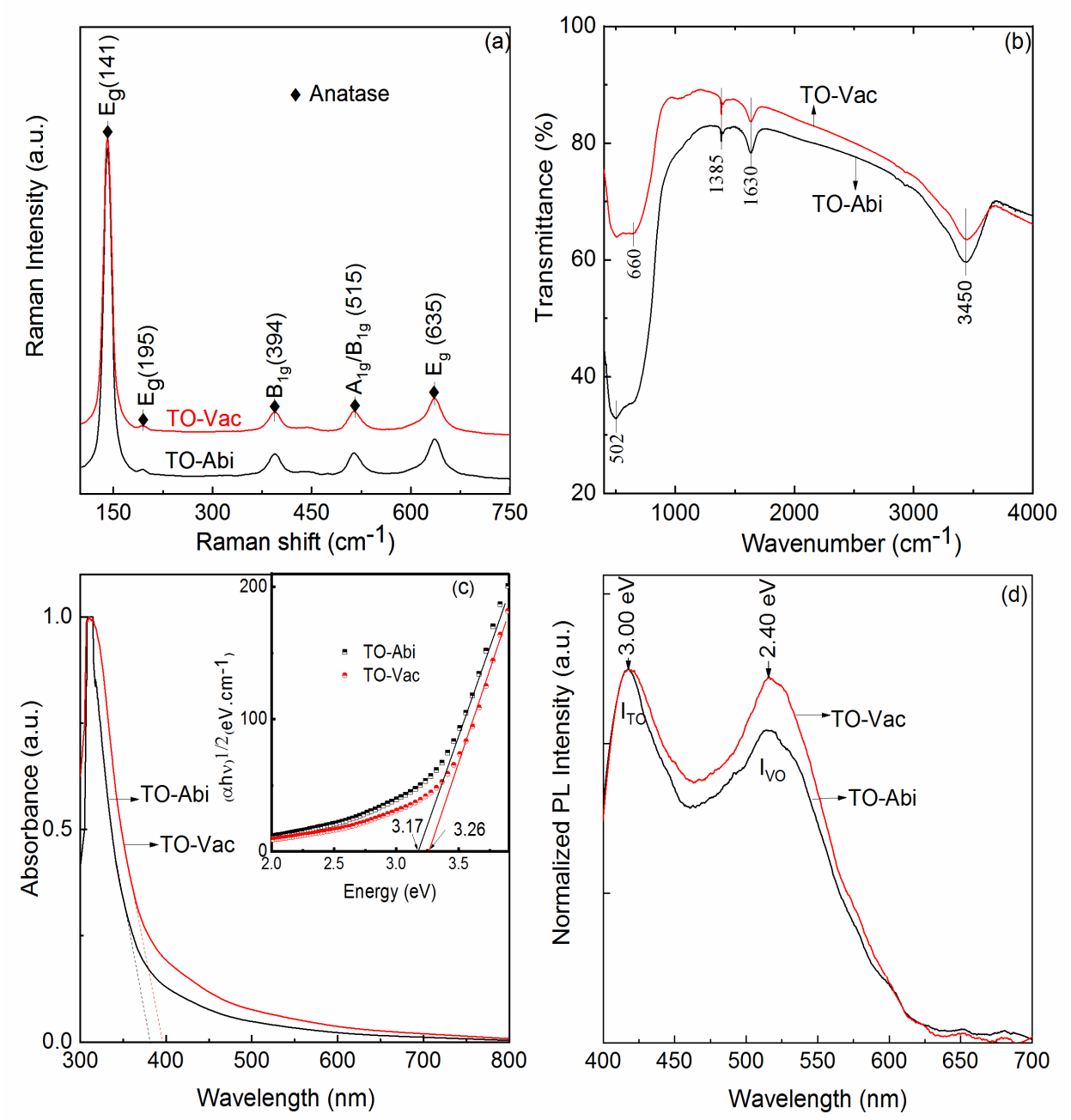

Fig. 3. (a) Raman spectrum, (b) Fourier transform infrared, (c) absorption, and (d) photoluminescence spectrum of TiO_2/FTO nanoparticle samples annealed at 450 °C in air and vacuum (~10^{-1} torr) for 100 min

$$Ti^{4+} + O^{2-} \leftrightarrow \frac{1}{2} O_2 + Ti^{3+} + 3e^- \quad (2)$$

$$2O^{2-} \leftrightarrow O_2 + V_o^{2+} + 2e^- \quad (3)$$

$$Ti^{4+} + e^- \rightarrow Ti^{3+} \quad (4)$$

The wide absorption peaks at 520 cm^{-1} and 660 cm^{-1} are caused by the stretching vibration of the Ti–O bond in the TiO_2 nanoparticles. The existence of organic functional groups (OH^-, C–OH) on the surface of TiO_2 during the annealing process might suggest active site for the reaction with a contamination coupling agent.

Fig. 3(c-d) presents the optical characteristics of TiO_2/FFO samples in the range from 300 to 800 nm at RT. The spectral absorptions were observed below the wavelength of 400 nm with absorption edges at 380 and 391 nm, which matches well with the reported semiconductor bandgap energy of the crystalline bulk anatase TiO_2 [20, 22, 36, 25, 43, 5, 30]. The energy bandgaps were evaluated as 3.26 eV and 3.17 eV by the Tauc's plot ($\left[F(R_\infty)h\nu\right]^{1/2}$, $n = 2$ *vs.* band energy, using the Kubelka–Munk model, as inset of Fig. 3(c)) for TO-Abi and TO-Vac samples, respectively [5, 44]. The absorption spectrum of both samples indicated the direct transition bandgaps [45]. The absorption edge of the TO-Vac sample shows a slight red shift towards the long wavelength, which is in a agreement with the photocatalyst activity of MO in the visible region. This phenomenon is attributed to the effect of modified energy electron density states (EDS) on the bottom of the

conduction band. There is low oxygen density during the annealing process (in vacuum conditions) leading to low EDS, which exhibits a shifting absorption edge to a long wavelength. To confirm that, we measured the photoluminescence (PL) spectrum of both samples in the range of 400-700 nm at RT, as seen in Fig. 3(d). The normalized intensity (I_{TO}) of PL spectra shows a peak at 413 nm (3.0 eV) for the bandgap transition of TiO_2, which is consistent with previous reports [5, 46]. While one emission peak at 516 nm (2.4 eV) is assigned to the transition band of oxygen vacancies (OVs) [47, 5]. The emission intensity (I_{OV}) peak at 516 nm of the TO-Vac sample is higher than that of the TO-Abi sample. However, the obtained PL spectrum is quite different compared to other reported PL spectrum below annealing temperature of 500 ^{o}C [47, 20, 37, 46, 21, 48]. It should be noted that this difference might be understood by different degrees of formation of oxygen vacancies, as well as quantum confinement effect *vs.* different sizes under synthesis conditions. Interestingly, we have compared the PL quantum efficiency of TiO_2 and evaluated the effect of vacuum on the contribution of oxygen vacancy to the spectral PL by the intensity between the PL peaks (I_{VO}/I_{TO}). If the ratio is increasing with high oxygen concentration, it indicates high VO density. Thus, it strongly suppresses the PL intensity due to high carrier recombination and trapping carrier density, which causes reduced photocurrent of the TiO_2 film-based PEC device. For detailed reduced quantum yield and VO density, and mechanism of PL emission spectra of TiO_2, we can reference other reports, elsewhere [47, 20, 21].

Fig. 4 presents the photoelectrochemical properties of the TiO_2/FTO electrodes under AM 1.5G illumination via three electrode system in a 1.0 M Kpi electrolyte. As seen in Fig 4 (a), all photoanodes showed a natural upward photocurrent density (*J*) *vs.* the applied potential likely *n*-type semiconductor behavior. That means photogenerated electrons in TiO_2/FTO electrode participate in the water reduction reaction to generate H_2 gas (*Equ. 5*) under illumination and applied potential.

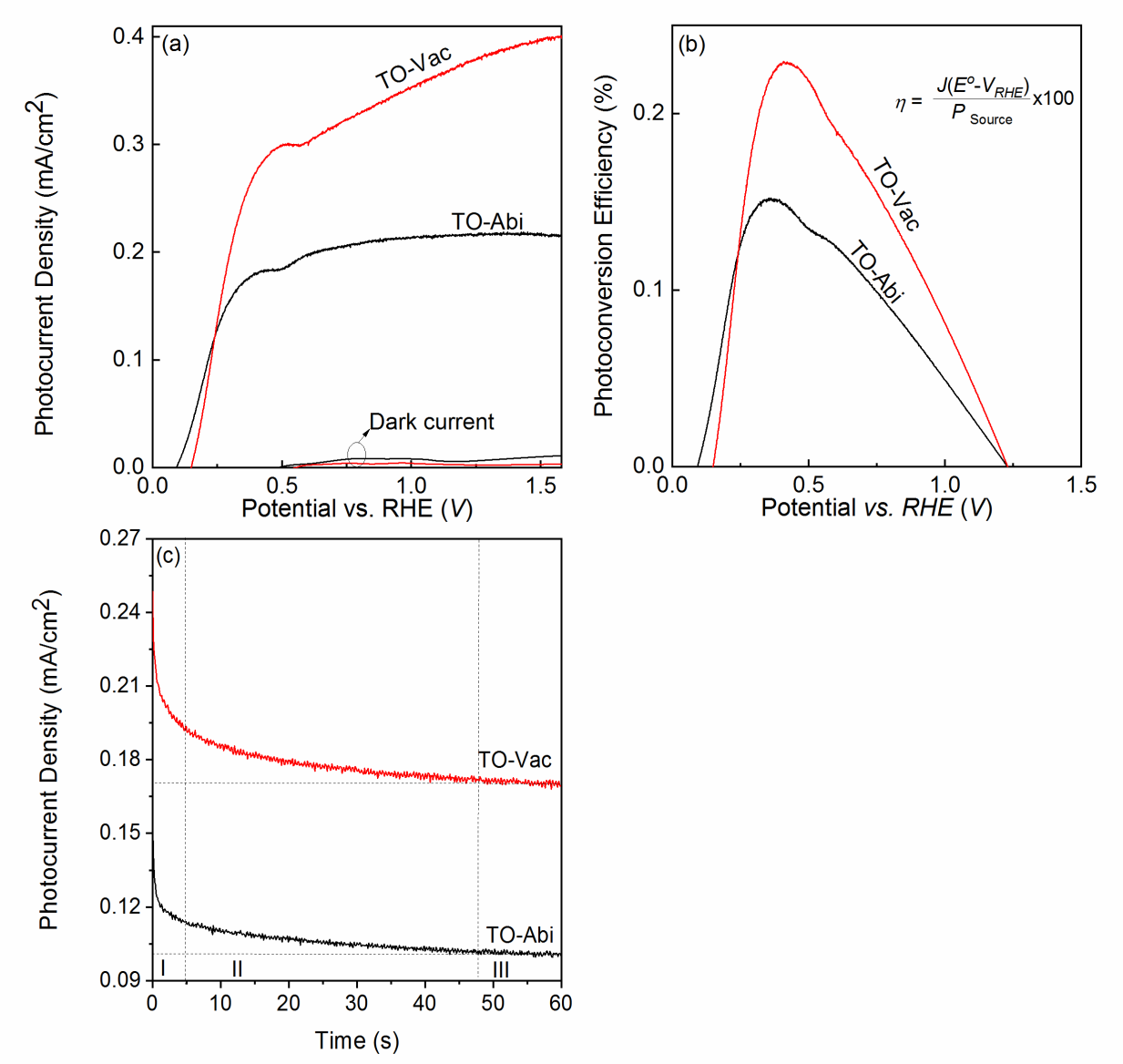

Fig. 4. (a) Linear sweep voltammograms (LSV) collection, (b) photoconversion efficiency evaluated from LVS curve and (c) comparing stability result for 1 min in both photoanodes, TO-Abi and TO-Vac samples.

The hole is transferred to the Pt electrode to participate in the water oxidation reaction to generate O_2 gas (*Equ. 6*)

$$2H^+ + 2e^- \rightarrow H_2 \quad (5)$$

$$2H_2O + 4h^+ \rightarrow O_2 + 4H^+ \quad (6)$$

The photocurrents increase from ca. 1.25 10^{-3} mA/cm^2 to 0.18 mA/cm^2 and 0.27 mA/cm^2 at 0.4 V (*vs. RHE*) due to the increase of separated photogenerated electrons for TO-Abi and TO-Vac samples, respectively. Then it saturates with the applied potential from 0.4 to 1.5 V due to the increase of photogenerated electrons, charge collection ability and improvement of charge transfer resistance of TiO_2 electrode. The photocurrent of the TO-Vac electrode (0.27 mA/cm^2) is higher than that of the TO-Abi electrode (0.18 mA/cm^2) at a potential of 0.4 *V* (*vs. RHE*). Significantly, the TO-Vac electrode exhibits PEC production performance with a positive onset potential of 0.15 *V* (*vs. RHE*) compared to the TO-Abi electrode (0.09 *V*). As mentioned above, the increasing photocurrent density of the TO-Vac sample is attributed to increasing active sites while the sample was annealed in a vacuum. Herein, we believe that the oxygen concentration rises, then increases the Fermi level of TiO_2, and thus, it increases the onset potential of the TiO_2 electrode. Therefore, we observed a shifting onset potential from 0.09 to 0.15 V (*vs. RHE*) when electrodes were annealed in air to vacuum.

Fig. 4(b) presents the photoconversion efficiency with the assumption of 100%. Faradaic efficiency of both PEC devices was evaluated by following *Equ.* 7 [4]

$$\eta(\%) = \frac{J(E_o - |V_{RHE}|)}{P_{source}} \times 100 \quad (7)$$

Where E_o = 1.23 V is the standard reversible potential, J is the photocurrent density (mA/cm^2), V_{RHE} is the bias potential *vs. RHE* (V), and P is the power density of incident light (mW/cm^2). As a result, the conversion efficiency of TO-Vac sample is 0.22%), which is higher than that of the TO-Abi electrode (η = 0.15%). In fact, due to a low oxygen concentration during the annealing process, OV density in anatase TiO_2 structure increases, in which if the carrier concentration is sufficient, the change in the concentration of carrier will no longer make the Fermi level increase, but instead strongly alter the dipole distribution in the Helmholtz layer at the interface of photoanode and electrolyte [20, 5, 21]. Also, when the OV concentration near the TiO_2 surface is high, it greatly increases the Schottky barrier height (SBH). Minor carriers are now blocked by the SBH and cannot be transferred to TiO_2 nanoparticles to contribute to the PEC current. Thus, the photoelectrocatalytic performance of the TO-Vac photoanodes was significantly enhanced in comparison with that of the TO-Abi photoanodes.

Besides that, we measured the stability of TiO_2/FTO samples in a 1.0 M Kpi electrolyte for 1 min, as seen in Fig. 4(c). The effect of pressure on the stability of TiO_2/FTO nanoparticles was investigated for three regions (*I, II*, and *III*). The response of both photoanodes indicated a similar slope in the range of 0–5 sec (I region) and 47–60 sec (III region). It can be explained that the photogenerated electrons of the *I* region are at

the same under illumination, because the loss energy of electron absorbance is neglected when they directly transfer from valence band to conduction band in a short time. For the *II* region, the photoelectrons generated and transferred to the conduction band are saturated, thus, the photocurrent is stable. On the contrary, the photocurrent response of TO-Vas electrode is slower than that of TO-Abi electrodes (region *II*). This reason is attributed to high OV concentration. Although OVs are present at the interface of the crystalline anatase TiO_2, those vacancies act as recombination centers only. Herein, photoelectrons are generated and trapped in defect centers, then reducing the lifetime of electrons. The mobile electrons interact with these charge defects and got scattered, and thereby the mobility decreases leading to low response. To clearly understand, we can reference other literature, elsewhere [20, 5, 21].

4. Conclusions

We investigated the synthesis of TiO_2/FTO (P25) nanoparticle electrodes by the spin-coating method using thermal annealing in air (TO-Abi sample) and in vacuum (TO-Vac sample) conditions. The optical characteristics of TiO_2/FTO samples were studied by using Raman, photoluminescence (PL), absorption, and FTIR techniques. The emission PL (516 nm) peak of oxygen vacancy of the TO-Vac sample showed high intensity and shifted towards a low energy bandgap of 3.17 eV compared to that of the TO-Abi sample (3.26 eV). Based on this result, the TiO_2-Vac photoelectrode obtained a photocurrent density of 0.27 mA/cm^2 and an energy conversion efficiency (η) of 0.22 % at 0.4 *V* (*vs. RHE*), which are higher than those of the TO-Abi electrode (0.18 mA/cm^2, 0.15%) due to

high oxygen vacancy density causing more active sites for photocatalyst. The positive onset potential of 0.15 *V* (*vs. RHE*) shifted towards 0.06 V compared to the TO-Abi electrode. This confirms the ability of oxygen vacancy on catalytic activity for a PEC application. This is further a promising approach to enhance photoelectrochemical water splitting efficiency of anatase crystalline TiO_2

Acknowledgement

This work was financially supported by Institute of Materials Science, Vietnam Academy of Science and Technology via the basic research project Code CS.12/20-21

Declaration of competing interest

The authors declare that they have no conflict of interest, and have not competed in this manuscript.

References

1. Bak, T., J. Nowotny, M. Rekas, and C.C. Sorrell, *Photo-electrochemical hydrogen generation from water using solar energy. Materials-related aspects,* Int. J. Hydrog. Energy, **27**(10) 991-1022 (2002)
2. Fujishima, A. and K. Honda, *Electrochemical Photolysis of Water at a Semiconductor Electrode,* Nature, **238**(5358) 37-38 (1972)
3. Grätzel, M., *Photoelectrochemical cells,* Nature, **414**(6861) 338-344 (2001)
4. Khan, S.U.M., M. Al-Shahry, and W.B. Ingler, *Efficient Photochemical Water Splitting by a Chemically Modified n-TiO_2,* Science, **297**(5590) 2243-2245 (2002)
5. Nguyen, T.-T., K.A. Dao, T.T.O. Nguyen, T.D.T. Ung, D.T. Nguyen, and S.H. Nguyen, *Unexpected impact of oxygen vacancies on photoelectrochemical performance of Au@TiO_2 photoanodes,* Mater. Sci. Semicond. Process., **127** 105714 (2021)
6. Ghosh, S. and P. Hajra, *6 - Metal oxide catalysts for photoelectrochemical water splitting*, in *Metal Oxide-Based Nanostructured Electrocatalysts for Fuel Cells, Electrolyzers, and Metal-air Batteries*, T.W. Napporn and Y. Holade, Editors. 2021, Elsevier. p. 105-138.
7. Kyesmen, P.I., N. Nombona, and M. Diale, *Heterojunction of nanostructured α-Fe_2O_3/CuO for enhancement of photoelectrochemical water splitting,* J. Alloy. Compd., **863** 158724 (2021)
8. Peleyeju, M.G. and E.L. Viljoen, *WO_3-based catalysts for photocatalytic and photoelectrocatalytic removal of organic pollutants from water – A review,* J. Water Process. Eng., **40** 101930 (2021)
9. Samuel, E., B. Joshi, M.-W. Kim, M.T. Swihart, and S.S. Yoon, *Morphology engineering of photoelectrodes for efficient photoelectrochemical water splitting,* Nano Energy, **72** 104648 (2020)
10. Zhang, Q., B. Zhai, Z. Lin, X. Zhao, and P. Diao, *CuO/$CuBi_2O_4$ bilayered heterojunction as an efficient photocathode for photoelectrochemical hydrogen evolution reaction,* Int. J. Hydrog. Energy (2021)
11. Singh, R. and S. Dutta, *A review on H_2 production through photocatalytic reactions using TiO_2/TiO_2-assisted catalysts,* Fuel, **220** 607-620 (2018)

12. Katoh, R., A. Furube, T. Yoshihara, K. Hara, G. Fujihashi, S. Takano, S. Murata, H. Arakawa, and M. Tachiya, *Efficiencies of Electron Injection from Excited N_3 Dye into Nanocrystalline Semiconductor (ZrO_2, TiO_2, ZnO, Nb_2O_5, SnO_2, In_2O_3) Films,* J. Phys. Chem. B, **108**(15) 4818-4822 (2004)
13. Schneider, J., M. Matsuoka, M. Takeuchi, J. Zhang, Y. Horiuchi, M. Anpo, and D.W. Bahnemann, *Understanding TiO_2 Photocatalysis: Mechanisms and Materials,* Chem. Rev., **114**(19) 9919-9986 (2014)
14. Jiang, Z., J. Zhu, D. Liu, W. Wei, J. Xie, and M. Chen, *In situ synthesis of bimetallic Ag/Pt loaded single-crystalline anatase TiO_2 hollow nano-hemispheres and their improved photocatalytic properties,* CrystEngComm, **16**(12) 2384-2394 (2014)
15. Maeda, K., *Photocatalytic properties of rutile TiO_2 powder for overall water splitting,* Catal. Sci. Technol., **4**(7) 1949-1953 (2014)
16. Ni, M., M.K.H. Leung, D.Y.C. Leung, and K. Sumathy, *A review and recent developments in photocatalytic water-splitting using TiO_2 for hydrogen production,* Renew. Sustain. Energy Rev., **11**(3) 401-425 (2007)
17. Shen, S., J. Chen, M. Wang, X. Sheng, X. Chen, X. Feng, and S.S. Mao, *Titanium dioxide nanostructures for photoelectrochemical applications,* Prog. Mater. Sci., **98** 299-385 (2018)
18. Tsukamoto, D., A. Shiro, Y. Shiraishi, Y. Sugano, S. Ichikawa, S. Tanaka, and T. Hirai, *Photocatalytic H_2O_2 Production from Ethanol/O_2 System Using TiO_2 Loaded with Au–Ag Bimetallic Alloy Nanoparticles,* ACS Catal., **2**(4) 599-603 (2012)
19. Malekshahi Byranvand, M., A. Nemati Kharat, L. Fatholahi, and Z. Malekshahi Beiranvand, *A Review on Synthesis of Nano-TiO_2 via Different Methods,* J. Nanostruct., **3**(1) 1-9 (2013)
20. Choudhury, B. and A. Choudhury, *Oxygen defect dependent variation of band gap, Urbach energy and luminescence property of anatase, anatase–rutile mixed phase and of rutile phases of TiO2 nanoparticles,* Physica E, **56** 364-371 (2014)
21. Santara, B., P.K. Giri, K. Imakita, and M. Fujii, *Evidence of oxygen vacancy induced room temperature ferromagnetism in solvothermally synthesized undoped TiO_2 nanoribbons,* Nanoscale, **5**(12) 5476-5488 (2013)
22. Cozzoli, P.D., E. Fanizza, R. Comparelli, M.L. Curri, A. Agostiano, and D. Laub, *Role of Metal Nanoparticles in TiO_2/Ag Nanocomposite-Based Microheterogeneous Photocatalysis,* J. Phys. Chem. B, **108**(28) 9623-9630 (2004)
23. Duan, Y., S. Zhou, Z. Chen, J. Luo, M. Zhang, F. Wang, T. Xu, and C. Wang, *Hierarchical TiO_2 nanowire/microflower photoanode modified with Au nanoparticles for efficient photoelectrochemical water splitting,* Catal. Sci. Technol., **8**(5) 1395-1403 (2018)
24. Zhang, P., T. Song, T. Wang, and H. Zeng, *Enhancement of hydrogen production of a Cu–TiO_2 nanocomposite photocatalyst combined with broad spectrum absorption sensitizer Erythrosin B,* RSC Adv., **7**(29) 17873-17881 (2017)
25. Li, W., R. Liang, A. Hu, Z. Huang, and Y.N. Zhou, *Generation of oxygen vacancies in visible light activated one-dimensional iodine TiO_2 photocatalysts,* RSC Adv., **4**(70) 36959-36966 (2014)
26. Tan, H., Z. Zhao, M. Niu, C. Mao, D. Cao, D. Cheng, P. Feng, and Z. Sun, *A facile and versatile method for preparation of colored TiO_2 with enhanced solar-driven photocatalytic activity,* Nanoscale, **6**(17) 10216-10223 (2014)
27. Kim, C.-S., B.K. Moon, J.-H. Park, B.-C. Choi, and H.-J. Seo, *Solvothermal synthesis of nanocrystalline TiO_2 in toluene with surfactant,* J. Cryst. Growth, **257**(3) 309-315 (2003)
28. Pardon, N., O. Omobola, M. Henry, T. Raymond, and Z. Simcelile, *Synthetic Methods for Titanium Dioxide Nanoparticles: A Review*, in *Titanium Dioxide - Material for a Sustainable Environment*, Y. Dongfang, Editor. 2018, Intech Open.
29. Kim, H., K. Noh, C. Choi, J. Khamwannah, D. Villwock, and S. Jin, *Extreme Superomniphobicity of Multiwalled 8 nm TiO_2 Nanotubes,* Langmuir, **27**(16) 10191-10196 (2011)
30. Oh, S.-M. and T. Ishigaki, *Preparation of pure rutile and anatase TiO_2 nanopowders using RF thermal plasma,* Thin Solid Films, **457**(1) 186-191 (2004)

31. Besra, L. and M. Liu, *A review on fundamentals and applications of electrophoretic deposition (EPD),* Prog. Mater. Sci., **52**(1) 1-61 (2007)
32. Francis, N. and A. Bernard, *Electrophoretic Deposition of Titanium Dioxide Thin Films for Photocatalytic Water Purification Systems,* Adv. Mater., **6**(4) 31-37 (2017)
33. Mehrotra, R.C. and A. Singh, *Recent Trends in Metal Alkoxide Chemistry*, in *Prog. Inorgan. Chem.* 1997. p. 239-454.
34. Oskam, G., A. Nellore, R.L. Penn, and P.C. Searson, *The Growth Kinetics of TiO_2 Nanoparticles from Titanium(IV) Alkoxide at High Water/Titanium Ratio,* J. Phys. Chem. B, **107**(8) 1734-1738 (2003)
35. Gablenz, S., D. Voltzke, H.P. Abicht, and J. Neumann-Zdralek, *Preparation of fine TiO_2 powders via spray hydrolysis of titanium tetraisopropoxide,* J. Mater. Sci. Lett., **17**(7) 537-539 (1998)
36. Huber, B., H. Gnaser, and C. Ziegler, *Electrical properties of nanocrystalline anatase TiO_2 thin films with different crystallite size,* Surf. Sci., **566-568** 419-424 (2004)
37. Nakamura, I., N. Negishi, S. Kutsuna, T. Ihara, S. Sugihara, and K. Takeuchi, *Role of oxygen vacancy in the plasma-treated TiO_2 photocatalyst with visible light activity for NO removal,* J. Mol. Catal. A-Chem., **161**(1) 205-212 (2000)
38. Ohsaka, T., F. Izumi, and Y. Fujiki, *Raman spectrum of anatase, TiO_2,* J Raman Spectrosc., **7**(6) 321-324 (1978)
39. Wyckoff, R.W.G., *Crystal Structures, Volume 1*. Vol. 1. 1965, New York: Interscience Publishers.
40. Araña, J., C. Garriga i Cabo, J.M. Doña-Rodríguez, O. González-Díaz, J.A. Herrera-Melián, and J. Pérez-Peña, *FTIR study of formic acid interaction with TiO_2 and TiO_2 doped with Pd and Cu in photocatalytic processes,* Appl. Surf. Sci., **239**(1) 60-71 (2004)
41. Erdem, B., R.A. Hunsicker, G.W. Simmons, E.D. Sudol, V.L. Dimonie, and M.S. El-Aasser, *XPS and FTIR Surface Characterization of TiO_2 Particles Used in Polymer Encapsulation,* Langmuir, **17**(9) 2664-2669 (2001)
42. Guo, G., Q. Shi, Y. Luo, R. Fan, L. Zhou, Z. Qian, and J. Yu, *Preparation and ageing-resistant properties of polyester composites modified with functional nanoscale additives,* Nanoscale Res. Lett., **9**(1) 215 (2014)
43. Mo, S.-D. and W.Y. Ching, *Electronic and optical properties of three phases of titanium dioxide: Rutile, anatase, and brookite,* Physical Review B, **51**(19) 13023-13032 (1995)
44. Shore, K.A., *Electronic Processes in Non-crystalline Materials*. Clarendon Press (Oxford and New York), ed. n. Ed. Vol. 55. 2014: Taylor & Francis. 337-337.
45. Mo, S.-D. and W.Y. Ching, *Electronic and optical properties of three phases of titanium dioxide: Rutile, anatase, and brookite,* Phys. Rev. B, **51**(19) 13023-13032 (1995)
46. Niederberger, M., M.H. Bartl, and G.D. Stucky, *Benzyl Alcohol and Titanium TetrachlorideA Versatile Reaction System for the Nonaqueous and Low-Temperature Preparation of Crystalline and Luminescent Titania Nanoparticles,* Chem. Mater., **14**(10) 4364-4370 (2002)
47. Abazović, N.D., M.I. Čomor, M.D. Dramićanin, D.J. Jovanović, S.P. Ahrenkiel, and J.M. Nedeljković, *Photoluminescence of Anatase and Rutile TiO_2 Particles,* J. Phys. Chem. B, **110**(50) 25366-25370 (2006)
48. Wang, X., S. Shen, Z. Feng, and C. Li, *Time-resolved photoluminescence of anatase/rutile TiO_2 phase junction revealing charge separation dynamics,* Chin. J. Catal., **37**(12) 2059-2068 (2016)